Eur. Phys. J. D (2023) 77:75
https://doi.org/10.1140/epjd/s10053-023-00650-4

THE EUROPEAN PHYSICAL JOURNAL D

Regular Article - Plasma Physics

Iterative kinetic model application in diagnostics of argon abnormal DC glow discharges

Djordje Spasojević[1,a], Nikola V. Ivanović[2,b], Nikodin V. Nedić[1,c], Milica Vasiljević[1,d], Nikola M. Šišović[1,e], and Nikola Konjević[1,f]

[1] Faculty of Physics, University of Belgrade, P.O. Box 44, 11001 Belgrade, Serbia
[2] Faculty of Agriculture, University of Belgrade, Nemanjina 6, 11080 Belgrade, Serbia

Received 20 November 2022 / Accepted 5 April 2023 / Published online 15 May 2023

Abstract. We report a study of the cathode sheath (CS) space of the argon glow discharges in the abnormal DC regime by means of the iterative kinetic model. By matching the model shapes of the side-on spectra with the experimental data for the Ar II 460.954 nm line obtained via optical emission spectroscopy, we have estimated the thickness of the CS space and the distributions of the electric field strength and gas temperature over the entire CS space of discharge.

1 Introduction

Glow discharge (GD) in abnormal regime occupies two characteristic spatial regions: cathode sheath (CS) and negative glow (NG). The CS space spreads from the cathode toward NG space and has a thickness of about 1 mm and an electric field strength distribution, which takes about 90% of discharge voltage. This distribution attains the maximum value of approximately 10 kV/cm near the cathode and afterward decreases reaching zero at the NG boundary, see [4, 29, 44]. Inside the CS, the electric field accelerates ions and electrons to the kinetic energy large enough for the realization of electron impact ionization of atoms, heavy particle excitation/ionization, and also sputtering of cathode atoms [4, 25, 29, 44]. Jointly with elastic collisions and energy transfer from the electric field, these inelastic collisions determine the distributions of ions and atoms and consequently their excitations leading to the emission of radiation having complex spectral shapes.

In our recent studies, we found that some argon ionic spectral lines, emitted out of abnormal DC GDs running at pressure values between 3 and 10 mbar, have such complex spectral profiles with excessively broadened pedestals, see [42]. Side-on recorded, these profiles are symmetric relative to the central wavelength showing expanded wings dominantly originated by the Doppler effect and negligibly by the DC Stark effect which is small for ionic lines.

To explain and describe the foregoing experimental findings, here we apply the iterative kinetic model to discharge in pure argon. The model, originally introduced for a description of the atomic lines in pure hydrogen GDs [38, 39], was recently adopted for application to the pure neon GDs [37], and here to discharges in pure argon, see [5] for an initial attempt.

The experimental part of our study is performed by the optical emission spectroscopy (OES) measurements of spectral profiles of argon atomic and ionic lines. The atomic lines were selected so that their estimated Stark shifts enable the determination of the electric field distributions measured so far by electric probes [3], deflection in CS of electron beam [23], fluorescence laser spectroscopy of Rydberg states [7], Den [10, 14, 15, 19], and using the optogalvanic effect [8, 9, 16, 27]). In this work, we used the Lo Surdo method for the electric field measurements [31] in which a photo plate is replaced by a CCD detector like in [17, 18, 24, 35, 37, 41], and the same method was earlier employed in the spectroscopic studies of hydrogen Balmer lines [1, 11, 13, 36, 40, 43, 45], and also in studies of helium lines [6, 20, 21, 26].

Guest editors: Bratislav Obradović, Jovan Cvetić, Dragana Ilić, Vladimir Srećković and Sylwia Ptasinska.

T.I. : Physics of Ionized Gases and Spectroscopy of Isolated Complex Systems: Fundamentals and Applications.

[a] e-mail: djordjes@ff.bg.ac.rs (corresponding author)
[b] e-mail: nikolai@ff.bg.ac.rs
[c] e-mail: nikodin.nedic@ff.bg.ac.rs
[d] e-mail: milica.vasiljevic@ff.bg.ac.rs
[e] e-mail: nikolas@ff.bg.ac.rs
[f] e-mail: nikruz@ff.bg.ac.rs

2 Experimental part of the study

We performed the measurements with the aid of the setup containing a Grimm GD source with a tungsten cathode. This source, made in our laboratory, has a longitudinal slot enabling side-on discharge observations at different distances from the cathode, see Ferreira, Human, and Butler for its original design [12], and Kuraica et al. [22] for its current version.

The discharges were realized in the 5–10 mbar range of pressure of argon gas (purity 99.999) at its flow of 300 cm^3/min and shown here only for the 5 mbar pressure used in most of the analytical applications because the lines become less resolved at higher pressures. We performed observations without a polarizer of the studied spectral lines using an Ebert-type spectrometer with 2 m focal length and with 651 g/mm reflection grating blazed at 1050 nm. The sensitivity of our spectrometer-radiation detector system was calibrated against a standard tungsten lamp showing maximum sensitivity in the wavelength range from 460 to 525 nm for recording in the second diffraction order. For this reason, we have selected the argon spectral lines (Ar II 460.954 nm and Ar I 522.127 nm) as the experimental basis for the current work. The measured instrumental profile of our system was approximately Gaussian with the full width at half maximum (FWHM) w_I of 8.2 pm in the second diffraction order. Other details regarding experimental procedure, which were the same as in the study [37] of a GD in pure neon, are presented in this reference including a schematic depiction of the setup.

3 Theoretical model

Prior to exposing the iterative kinetic model, we qualitatively illustrate the most relevant CS processes leading to the formation of the weakly ionized argon gas that emits the radiation whose spectroscopic profiles are recorded in our experiment. Due to the plane cathode and small (˜ 1 mm) thickness of the CS under our discharge conditions, the system can be considered as one having distributions of relevant quantities (e.g., of the electric field) that depend only on the distance from the cathode, like is taken in [37], for a similar model in hydrogen see [28, 39].

Most of the singly charged ions are generated by electron impact on the parent atoms. As the atoms are (mostly) cold, the so-generated ions are cold as well due to small momentum transfer in collision with electrons. Some of the ions that originated in the NG region diffuse into the CS and, together with the ions generated in the CS, are accelerated by the electric field toward the cathode making this direction a dominant direction of ions' motion.

Traveling to the cathode, the (positive) ions occasionally undergo in collisions. Because the number densities of electrons and ions in a weakly ionized gas are by several orders of magnitude smaller than for the matrix gas atoms, and due to the largest cross sections, the greatest effects on the distribution of positive ions have the momentum transfer collisions with the matrix gas and the charge exchange collisions, $A^+ + B \rightarrow A + B^+$, resulting in a production of a fast atom A and a slow ion B^+. Besides these collisions for the formation of the line shape essential are the excitations of ions leading to the emission of the ionic spectral lines. When observed side-on, this radiation gives profiles that are symmetric relative to the central wavelength. On the other hand, the pedestals of the end-on profiles are broadened more to the red than to the blue side showing that more Ar^+ ions are moving toward the cathode (i.e., away from the end-on observer), which is illustrated in Fig. 1b.

Accelerated by the electric field, positive ions arrive at the cathode with the average kinetic energy (e.g., 100 eV) that is of the same order of magnitude as the maximum energy attainable in the CS (e.g., ˜ 600 eV). Once inside the cathode, most of the incoming fast ions are neutralized and due to collisions randomly move inside the cathode. Part of the ions leaves the cathode as the backscattered fast atoms, while the rest stay inside (wherefrom some of them are sputtered at some later time like the atoms of the cathode material).

After returning into the cathode sheath, some of the backscattered atoms are ionized and if excited contribute by their radiation to the spectra of ionic lines. However, our Monte Carlo simulations, performed by the SRIM software package [47], see also [30, 32–34, 46], show that they retain at most 60% of the kinetic energy of their parent ions, see Fig. 2, which they rapidly loose in the collisions with matrix gas. At such energies, the probability for their ionization in collisions with the atoms of the matrix gas is rather small according to the cross section data from [2]. As the number densities of other ionization agents are small, the remaining ionization channels are even less probable and, therefore, the (indirect) contribution to the ionic radiation coming from the fast backscattered Ar atoms can be considered as negligible in our case.

In general, the bombardment by fast ions and atoms may cause the sputtering of the cathode atoms which spread through the discharge forming the matrix gas together with the atoms of discharge gas. In the case of discharges in hydrogen, mentioned in the Introduction, the amount of sputtering is negligible due to very small mass of hydrogen. Here, however, like in the case of neon GD, the sputtering exists (see the W lines in Fig. 1 and sputtering data in Fig. 3) caused by a considerable mass of argon projectiles. The presence of sputtered W atoms turns out to be important for building the profiles of the argon spectral lines, because the largest Doppler shifts visible in the side-on profiles could not be attained without their presence as the scattering centers; for more details, see [37].

The stationary state of a DC GD in argon is achieved in a balance of the elementary processes taking place in the discharge. The iterative kinetic model includes the

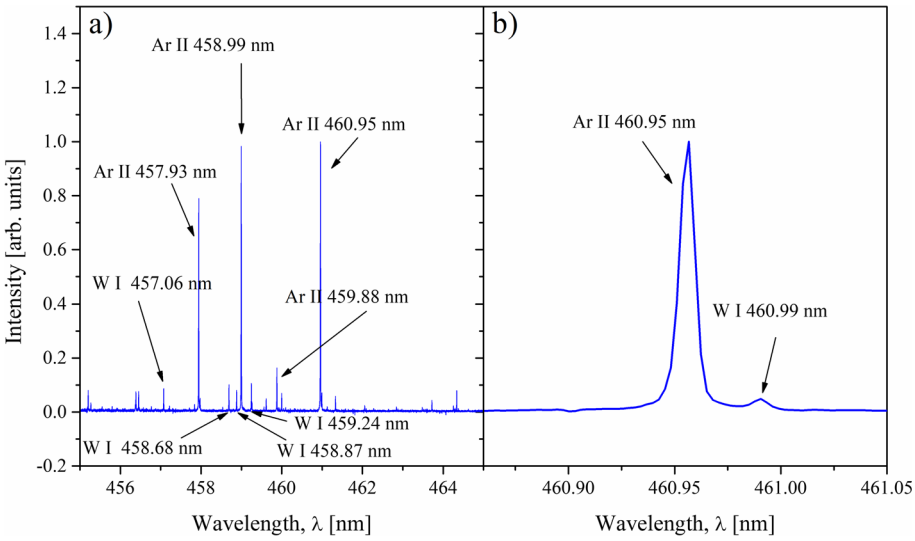

Fig. 1 **a** Radiation intensity versus wavelength λ for a portion of the end-on spectra containing several argon ionic lines together with several lines emitted by the sputtered tungsten atoms. The spectrum is recorded in a pure Ar GD operated with tungsten cathode at p = 4.5 mbar, V = 650 V, and I = 12 mA. **b** Zoomed part of **a** showing the end-on profile of ionic argon spectral line with 460.954 nm central wavelength; note that W I 460.99 nm spectral line is also visible here, as well as in Figs. 5 and 6

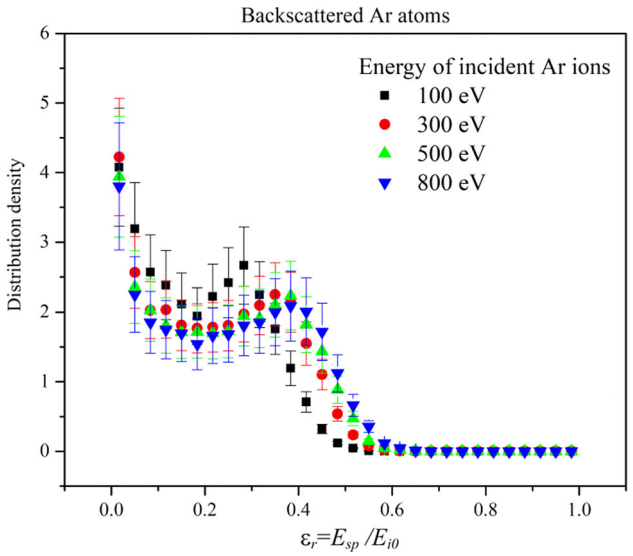

Fig. 2 Distribution density of backscattered Ar atoms shown against their relative energy $\varepsilon_r = E_{bs}/E_{i0}$. ($E_{bs}$ is the energy of the backscattered Ar atom, and E_{i0} is the energy of the incident Ar ion.) The distribution is obtained in SRIM simulations for 10 mm tungsten layer and perpendicular incidence of argon ions with energies quoted in legend. For better visibility, the uncertainties are magnified 2 times

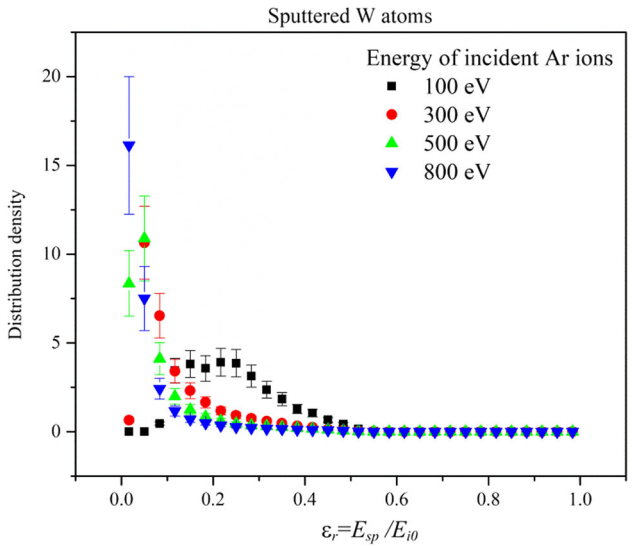

Fig. 3 Distribution density of sputtered W atoms as a function the their relative energy $\varepsilon_r = E_{\rm sp}/E_{i0}$. ($E_{\rm sp}$ is the energy of the sputtered W atom, and E_{i0} is the energy of the incident Ar ion.) The distributions are obtained in the same set of SRIM simulations as shown in Fig. 2. For better visibility, the uncertainties are magnified 2 times

most relevant of them through the equations

$$\vec{v}\cdot\frac{\partial f_{\rm Ar^+}}{\partial\vec{r}}+\frac{e\vec{E}}{m_{\rm Ar}}\cdot\frac{\partial f_{\rm Ar^+}}{\partial\vec{v}}=I_{\rm Ar^+}(\vec{r},\vec{v}), \quad (1)$$

$$\vec{v}\cdot\frac{\partial f_e}{\partial\vec{r}}-\frac{e\vec{E}}{m_e}\cdot\frac{\partial f_e}{\partial\vec{v}}=I_e(\vec{r},\vec{v}), \quad (2)$$

$$\vec{v}\cdot\frac{\partial f_{W^+}}{\partial\vec{r}}+\frac{e\vec{E}}{m_W}\cdot\frac{\partial f_{W^+}}{\partial\vec{v}}=I_{W^+}(\vec{r},\vec{v}), \quad (3)$$

$$\frac{\partial}{\partial\vec{r}}\cdot\vec{E}=\frac{e}{\varepsilon_0}(n_{\rm Ar^+}+n_{\rm W^+}-n_e), \quad (4)$$

similarly to the case of GDs in hydrogen and neon GDs [37–39]. In these equations, $m_{\rm Ar}$ is the mass of argon and m_W of tungsten atom, m_e is the mass of electron, e is the elementary charge, and ε_0 is the vacuum permittivity, while $\vec{v}$ and $\vec{r}$ are velocity and position vectors, respectively. Equation (1) is the kinetic equation for the distribution $f_{\rm Ar^+}(\vec{r},\vec{v})$ of the singly charged positive argon ions,

Ar^+, with collision integral $I_{A^+}(\vec{r},\vec{v})$. Likewise, $f_e(\vec{r},\vec{v})$, $I_e(\vec{r},\vec{v})$ are their correspondings for the electrons in Eq. (2), and $f_{W^+}(\vec{r},\vec{v})$, $I_{W^+}(\vec{r},\vec{v})$ for the W ions in Eq. 3. Equation 4 is the Maxwell's equation for the electric field $\vec{E}(\vec{r})$ in which $\rho(\vec{r}) = e[n_{Ne^+}(\vec{r}) + n_{A^+}(\vec{r}) - n_e(\vec{r})]$ is the charge density; n_{Ar^+}, n_{W^+}, and n_e are the number densities of Ar ions, W ions, and electrons.

The foregoing system of equations is not closed as it implicitly involves distribution density functions of Ar atoms and W atoms. Because the majority of these atoms are cold, we for simplicity assume that they are locally thermalized so that their distribution density functions read

$$f_A(\vec{r},\vec{v}) = n_A(m_A/2\pi k_B T)^{3/2}\exp\left(-m_A v^2/2k_B T\right), \tag{5}$$

$$f_W(\vec{r},\vec{v}) = n_W(m_W/2\pi k_B T)^{3/2}\exp\left(-m_W v^2/2k_B T\right), \tag{6}$$

being specified by constant number densities n_A and n_W, zero velocity of macroscopic motion, $\vec{u}(\vec{r}) = \int \vec{v} f(\vec{r},\vec{v}) d^3\vec{v}/n = 0$, and $T(z) \approx T_0 + zT'$ as the temperature distribution that is the same for both types of atoms linearly depending on the distance z from the cathode. (T_0 is the temperature, and T' is its gradient at the cathode.)

Proceeding with further simplifications, we keep just the dominant collision integrals describing:

- (symmetric) charge and momentum transfer for argon atoms and ions

$$Ar^+ + Ar \rightarrow \text{(fast) Ar} + \text{(slow) } Ar^+, \tag{7}$$

$$Ar^+ + Ar \rightarrow \text{Momentum Transfer}, \tag{8}$$

- (asymmetric) charge and momentum transfer for argon ions and tungsten atoms

$$Ar^+ + W \rightarrow \text{(fast) Ar} + \text{(slow) } W^+, \tag{9}$$

$$Ar^+ + W \rightarrow \text{Momentum Transfer}. \tag{10}$$

- (asymmetric) charge and momentum transfer for tungsten ions and argon atoms

$$W^+ + Ar \rightarrow \text{(fast) } W + \text{(slow) } Ar^+, \tag{11}$$

$$W^+ + Ar \rightarrow \text{Momentum Transfer}, \tag{12}$$

- and (symmetric) charge and momentum transfers for tungsten ions and atoms

$$W^+ + W \rightarrow \text{(fast) } W + \text{(slow) } W^+, \tag{13}$$

$$W^+ + W \rightarrow \text{Momentum Transfer}. \tag{14}$$

For (7) and (8), we used the cross sections from [2], and for (9)–(14), we employed model cross sections as in [37], while all differential cross sections are as in collisions of hard spheres.

Previously listed equations enable a self-consistent determination of the electric field and argon ion distributions. While the former is directly comparable with the experimental data, the ion distribution was not directly measurable in our experiment. Instead, spectral profiles of the selected ionic line, emitted by the excited Ar ions, $(Ar^+)^*$, were recorded as its indirect consequence. These excitations take place in collisions with Ar atoms:

$$Ar^+ + Ar \rightarrow \left(Ar^+\right)^* + Ar, \tag{15}$$

and with W atoms:

$$Ar^+ + W \rightarrow \left(Ar^+\right)^* + W, \tag{16}$$

while the electron impact excitation:

$$e + A^+ \rightarrow e + \left(A^+\right)^*, \tag{17}$$

may be neglected because the electrons have much smaller number density than the matrix gas atoms. Regarding the excitation, we used [2] data for the cross section $\sigma^{(exc)}_{Ar^+\text{-}Ar}$, whereas for (16) we took that the cross section $\sigma^{(exc)}_{Ar^+\text{-}W}$ depends on the argon ion's kinetic energy E_k as

$$\sigma^{(exc)}_{Ar^+-W}(E_k) \propto \sigma^{(exc)}_{Ar^+-W}(E_k)/E_k^{\alpha}, \tag{18}$$

with exponent $\alpha = 2.6$ providing matching to the experimental data, see [37].

Finally, we described the ionization of Ar and W atoms following [37], cf. Equations (27) and (28) in [37], and employed the approximate symmetry of relevant CS quantities, which transformed our equations into a system of 1D discrete equations that we iteratively solved using the procedure explained in [37].

4 Results

Here, we show the forecast of the iterative kinetic model regarding the data measured in the pure argon glow discharge operated at pressure $p = 4.5$ mbar, voltage $V = 650$ V, and current $I = 12$ mA. The presented experimental profiles of the Ar II 460.954 nm ionic spectral line, whose spectroscopic data are given in Table 1, are averages of 10 successive recordings performed in a single stationary discharge. The uncertainties are calculated as $\varepsilon_{tot} = \sqrt{\varepsilon^2_{sys} + \varepsilon^2_{rnd}}$ using detector systematic error ε_{sys} and the statistical error ε_{rnd} taken at the standard deviation 95% confidence level. For all experimental data, shown in this section, the predictions of

Table 1 Spectroscopic data for the studied ionic Ar II spectral line taken from NIST https://physics.nist.gov/PhysRefData/ASD/lines_form.html

	Wavelength [nm]	Lower level E_i, Configuration, Term, J	Upper level E_j, Configuration, Term, J	E_i [cm^{-1}]	E_j [cm^{-1}]
Ar II	460.954	$3s^2 3p^4(^1\mathrm{D})\ 4s^2\mathrm{D}$ 7/2	$3s^2 3p^4(^1\mathrm{D})\ 4p^2\mathrm{F}^\circ$ 7/2	148 842.47	170 530.40

Table 2 The set of model parameter values giving the best matching with all experimental profiles shown in Figs. 4, 5 and 6

Model parameter	Value
Cathode sheath thickness, d_{CS}	(0.84 ± 0.7) mm
Gas temperature at the cathode surface, T_0	(590 ± 80) K
Gradient of gas temperature, T'	(70 ± 50) K/mm
Effective cross section for the ionization of Ar atoms by electron impact, $\sigma^{(\mathrm{eff})}_{e,\mathrm{A}+}$	$(2.2 \pm 0.3)\times10^{-20}$ m^2
Effective cross section for the ionization of sputtered atoms by electron impact, $\sigma^{(\mathrm{eff})}_{e,\mathrm{W}+}$	$(1.6 \pm 0.3)\times10^{-20}$ m^2
Number density of Ar^+ ions at the CS-NG boundary, $n^0_{\mathrm{A}+}$	$(1.3 \pm 0.2)\times10^{18}$ m^{-3}
Number density of W ions at the CS-NG boundary, $n^0_{\mathrm{W}+}$	$(1.5 \pm 0.5)\times10^{17}$ m^{-3}
Fraction N_W/N_{tot} of sputtered W atoms in the CS	0.3 ± 0.1

the model are found using the single set of parameter values quoted in Table 2 providing best matching with the experimental data.

In Fig. 4, we show the experimental electric field distribution determined according to the procedure from [41] using measured Stark shifts of the atomic line Ar I 522.127 nm side-on spectra recorded together with the Ar II 460.954 nm line profiles. The theoretical prediction for this distribution, obtained with the aid of our model, is calculated for the parameters from Table 2 and shown by the full (red) line.

In Fig. 5, we present the model prediction for the Ar II 460.954 nm spectral line experimental side-on profile at the distance $d = 0.125$ mm from the cathode where the electric field strength is 13.2 kV/cm. The profile manifests excessively broadened wings emitted by ions having with large velocities along the side-on direction. Such velocities are result of a collision of ion either with (cold) Ar or W atoms; their contributions to the overall line profile are shown by thin lines in Fig. 5 as is indicated in the legend. The peak at the center of the profile is formed by the radiation of the Ar^+ ions mostly those with small energy. Such ions originate from (cold) Ar atoms ionized by electrons, and they contribute to the overall profile by the amount presented by the thin (green) line in Fig. 5.

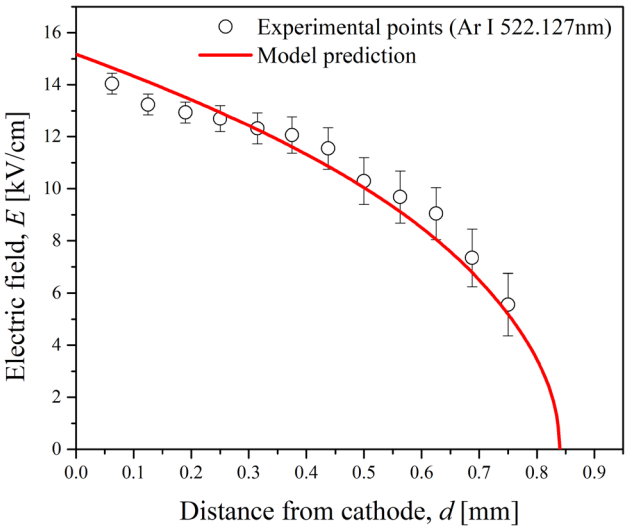

Fig. 4 Distribution of the electric field, E, in a function of distance from the cathode, d, in pure Ar discharge operated at $p = 4.5$ mbar, $V = 650$ V, and $I = 12$ mA. and $V = 650$ V. The experimental electric field distribution is shown by symbols and the model curve by the full line

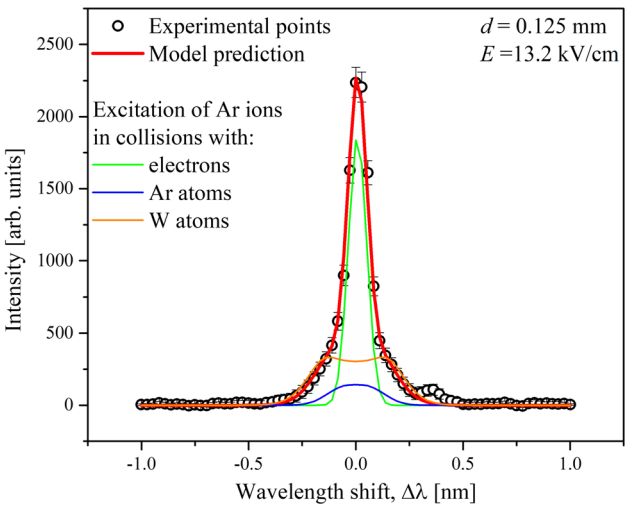

Fig. 5 Side-on spectral profile of the Ar II 460.954 nm line taken 0.125 mm from the cathode. Experimental points are presented by symbols, see in [42], and the full (thick) line shows the model profile for the parameters from Table 2. Thin lines show the parts due to the argon ion excitation by electrons, and by argon and tungsten atoms

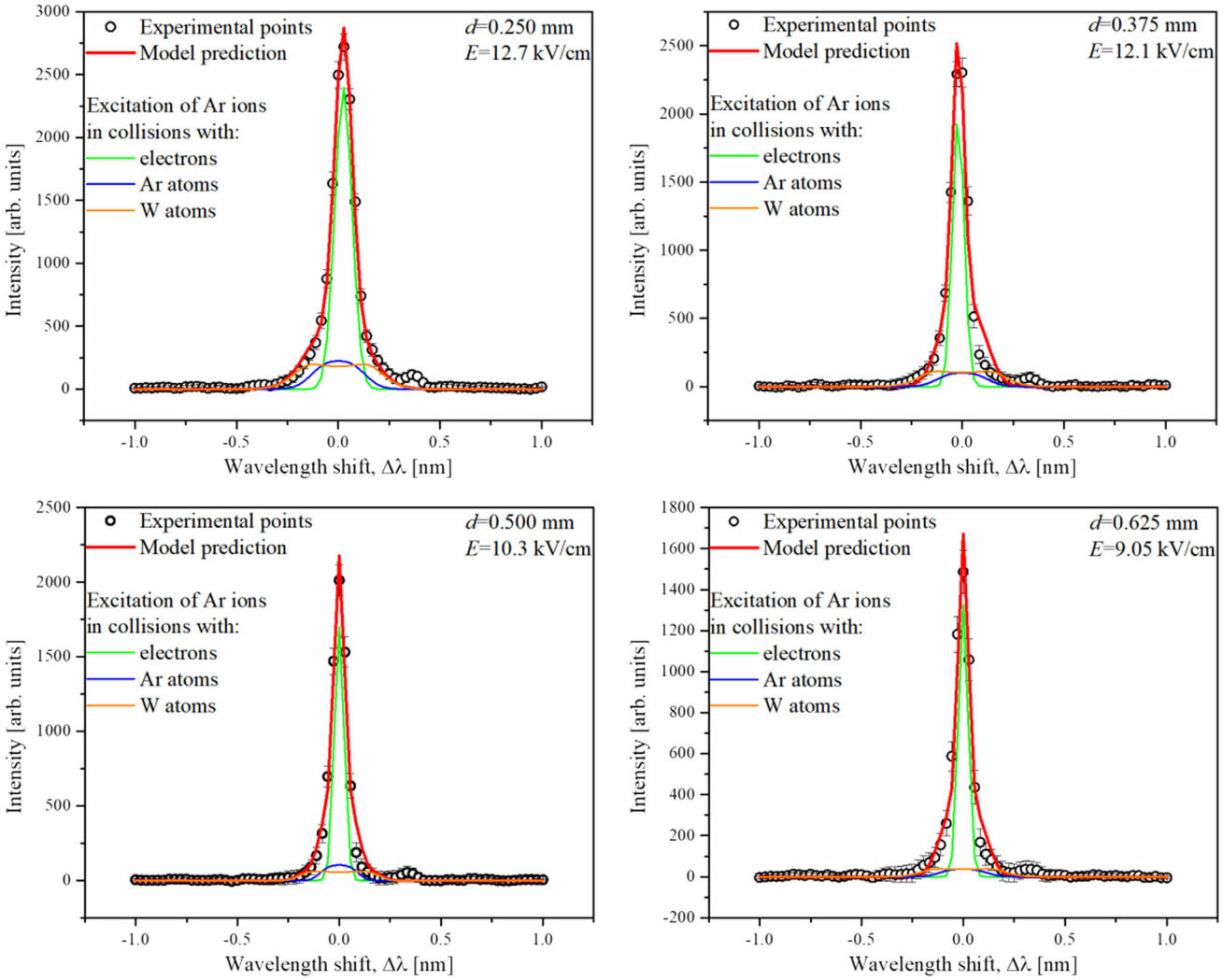

Fig. 6 Experimental Ar II 460.954 nm side-on profiles (shown by points) together with the (thick) full line, showing the corresponding model predictions for the overall line shape, and the (thin) full lines depicting different excitations specified in legend. The profiles are taken at four positions d from the cathode, given by distance d jointly with electric field E

Points and uncertainty bars present in Fig. 6 the experimental profiles of the same spectral line taken at additional four different positions (see the legend) spanning almost the whole CS of discharge. What one can see is that the width of the wings becomes smaller with the increase in cathode distance, whereas the central peak becomes more and more pronounced.

5 Discussion and conclusion

In this paper, we report a study of the glow discharge cathode sheath (CS) region in pure argon in which we, using the iterative kinetic model, predicted the profile of a selected ionic argon spectral line and estimated the electric field and temperature distribution together with CS thickness. These predictions are obtained using a dedicated computer program minimizing the deviations between theoretical predictions and experimental data simultaneously for all experimental spectral profiles recorded in the same discharge. Our program does this job typically in about 30 min which is much less then time needed for the Monte Carlo simulations.

In our previous studies, we have analyzed with the aid of the iterative kinetic model the cathode sheath of discharges in pure hydrogen [38, 39] and in pure neon [17, 37], whereas in this paper the scope of the model application is extended to the discharges in pure argon. Our findings show that the spectral lines emitted by argon ions also have wings that are excessively broadened which was experimentally observed/reported in [42] and theoretically analyzed in this paper in the case of Ar II 460.954 nm spectral line profiles recorded at 4.5 mbar pressure; with an exception of the experimental profile from Fig. 5, all other data in this article are not published elsewhere. As the Stark effect for the ionic lines is small, the broadening is caused dominantly by

the Doppler effect due to large velocities in the observation direction of the fast-emitting ions scattered in collisions with the argon and sputtered tungsten atoms. Similarly as argued in [37], we conclude here that in the formation of the line wings an important role is played by the scattering on tungsten atoms because the scattered argon ions get in the observation direction at most quarter of their incident kinetic energy in scattering on argon atoms, but as large as 80% in scattering on tungsten atoms, which is comparably less than in the neon case due to two times greater mass of argon than neon ions. In this way, the formation of wings of the monitored ionic spectral lines in both argon and neon discharges is substantially different from the case of discharge in pure hydrogen where the sputtering is small and the shapes of studied atomic lines emitted by the fast atoms, moving both toward and away from the cathode due to significant backscattering, show considerable Stark together with Doppler broadening, see [38].

At the end of this study, let us point out that for a proper application of the model the knowledge of the relevant cross section is necessary. This was only partially the case here, so for the absent ones we assumed to be proportional to the known data for similar processes and chose the factor of proportionality so to achieve a reasonable agreement with our experimental profiles. Considering this, the reported model values should be considered with prudence.

Acknowledgements This work was supported by the Ministry of Education, Science, and Technological Development of the Republic of Serbia (Grant No. 451-03-47/2023-01/200162).

Author contributions

DS contributed to conceptualization, methodology, investigation, and writing—original draft. NVI was involved in conceptualization, investigation, and writing—review. NVN contributed to conceptualization, investigation, and writing—review. MV was involved in conceptualization, investigation, and writing—review. NŠ contributed to conceptualization, methodology, and investigation. NK was involved in conceptualization, methodology, writing—review, and supervision.

Data Availability This manuscript has associated data in a data repository. [Authors' comment: The datasets supporting the conclusions of this article are available from the corresponding author upon reasonable request.]

Declarations

Conflict of interest The authors declare that they have no known competing financial interests or personal relationships that could have appeared to influence the work reported in this paper.

References

1. C. Barbeau, J. Jolly, Electric field measurement in the cathode sheath of a hydrogen glow discharge. Appl. Phys. Lett. **58**(3), 237–239 (1991)
2. A. Bogaerts, R. Gijbels, Comparison of argon and neon as discharge gases in a direct-current glow discharge a mathematical simulation. Spectrochim. Acta B **52**(5), 553–565 (1997)
3. W.L. Brown, E.E. Thompson, XCVIII. The potential distribution across the cathode dark space. London Edinb. Dublin Philos. Mag. J. Sci. **8**(53), 918–942 (1929)
4. B. Chapman, Glow discharge processes: sputtering and plasma etching. Phys. Today **34**, 62 (1980)
5. M. Cvejić, Dj. Spasojević, N.M. Šišović, N. Konjević, A contribution to spectroscopic diagnostics and cathode sheath modeling of micro-hollow gas discharge in argon. J. Appl. Phys. **110**, 033305 (2011)
6. N. Cvetanović, M.M. Martinović, B.M. Obradović, M.M. Kuraica, Electric field measurment in gas discharcges using startk shifts of He I lines and their forbiden counterparts. J. Phys. D Appl. Phys. **48**(20), 205201 (2015)
7. U. Czarnetzki, D. Luggenhölscher, H. Döbele, Sensitive electric field measurment by fluorescence-dip spectroscopy of rydberg states of atomic hydrogen. Phys. Rev. Lett. **81**(21), 4592–4595 (1998)
8. M.I. de la Rosa, C. Pérez, K. Grützmacher, L.M. Fuentes, Electric field strenghts in hollow cathode measured by Doppler-free two photon optogalvanic spectroscopy via Stark splitting of the 2S level of deuterium. Plasma Sources Sci. Technol. **18**(1), 015012 (2008)
9. M.I. de la Rosa, C. Pérez, K. Grützmacher, A. Gonzalo, A. Steiger, Electric field measurments in hollow cathode discharge by two-photon polarization spectroscopy of atomic deuterium. Plasma Sources Sci. Technol. **15**(1), 105–111 (2006)
10. E.A. Den Hartog, D.A. Doughty, J.B. Lawler, Laser optogalvanic and fluorescence studies of the cathode region of a glow discharge. Phys. Rev. A **38**(5), 2471–2491 (1988)
11. Z. Donkó, K. Rózsa, R.C. Tobin, K.A. Peard, Modeling and measurements on an obstructed glow discharge in helium. Phys. Rev. E **49**(4), 3283–3289 (1994)
12. N.P. Ferreira, H.G.C. Human, L.R.P. Butler, Kinetic temperatures and electron densities in the plasma of a side view Grimm-type glow discharge. Spectrochim. Acta Part B **35**(5), 287–295 (1980)
13. B.N. Ganguly, A. Garscadden, Electric field and Doppler emission profile measurements in an obstructed hydrogen discharge. J. Appl. Phys. **70**(2), 621–627 (1991)
14. B.N. Ganguly, J.R. Shoemaker, B.L. Preppernau, A. Garscadden, Rydberg state Stark spectroscopic measurement of electric-field profile in a glow discharge. J. Appl. Phys. **61**(8), 2778–2783 (1987)
15. V.P. Gavrilenko, H.J. Kim, T. Ikutake, J.B. Kim, Y.W. Choi, M.D. Bowden, K. Muraoka, Measurement method for electric fields based on Stark spectroscopy of argon atoms. Phys. Rev. E **62**(5), 7201–7208 (2000)
16. V. Gonzalez-Fernandez, K. Grützmacher, C. Peréz, M.I. de la Rosa, Influence of the cathode material in

the cathode fall characteristics of a hydrogen hollow cathode glow-discharge. J. Appl. Phys. **124**(3), 033302 (2018)
17. N.V. Ivanović, N.V. Nedić, N.M. Šišović, Dj. Spasojević, N. Konjević, Ne II spectral lines in the cathode sheath of an abnormal glow discharge. Eur. Phys. J. D **75**, 26 (2021)
18. N.V. Ivanović, N.M. Šišović, Dj. Spasojević, N. Konjević, Measurement of the DC Stark shift for visible NeI lines and electric field distribution in the cathode sheath of an abnormal glow discharge. J. Phys. D Appl. Phys. **50**(12), 125201 (2017)
19. T. Kampschulte, J. Schulze, D. Luggenhölscher, M.D. Bowden, U. Czarnetzki, Laser spectroscopic electric field measurement in krypton. New J. Phys. **9**(1), 18 (2007)
20. M.M. Kuraica, N. Konjević, Electric field measurement in the cathode fall region of a glow discharge in helium. Appl. Phys. Lett. **70**(12), 1521–1523 (1997)
21. M.M. Kuraica, N. Konjević, I.R. Videnović, Spectroscopic study of the cathode fall region of Grimm-type glow discharge in helium. Spectrochim. Acta Part B **52**(6), 745–753 (1997)
22. M. Kuraica, N. Konjević, M. Platiša, D. Pantelić, Plasma diagnostics of the Grimm-type glow discharge. Spectrochim. Acta Part B **47**(10), 1173–1186 (1992)
23. P.F. Little, A.V. von Engel, The hollow-cathode effect and the theory of glow discharges. Proc. R. Soc. London Ser A **224**(1157), 209–227 (1954)
24. G.L. Majstorović, N.V. Ivanović, N.M. Šišović, S. Djurović, N. Konjević, Ar I and Ne I spectral line shapes for an abnormal glow discharge diagnostics. Plasma Sources Sci. Technol. **22**(4), 045015 (2013)
25. R.K. Marcus, J.A.C. Broeckaert, *Glow discharge plasmas in analytical spectroscopy* (John Wiley & Sons Ltd, Chichester, 2003)
26. B.M. Obradović, N. Cvetanović, S.S. Ivković, G.B. Sretenović, V. Kovačević, I.B. Krstić, M.M. Kuraica, Methods for spectroscopic measurement of electric field in atmospheric pressure helium discharges. Eur. Phys. J. Appl. Phys. **77**(3), 30802 (2017)
27. C. Pérez, M.I. de la Rosa, K. Grützmacher, Hollow cathode fall field strength measured by Doppler-free two-photon optogalvanic spectroscopy via Stark splitting of the 2S level of hydrogen. Eur. Phys. J. D **56**(3), 369–375 (2010)
28. A.V. Phelps, Energetic ion, atom, and molecule reactions and excitation in low-current H2 discharges: model. Phys. Rev. E **79**, 066401 (2009)
29. Y.P. Raizer, J.E. Allen, *Gas discharge physics* (Springer, Berlin, 1997)
30. R. Ramos, G. Cunge, M. Touzeau, N. Sadeghi, Absorption spectroscopy in BCl_3 inductively coupled plasmas: determination of density, rotational, translational and vibrational temperatures of BCl molecule. J. Phys. D Appl. Phys. **41**(11), 115205 (2008)
31. N., Ryde, Atoms and molecules in electric fields. (Stockholm, Almqvist & Wiksell International,1976)
32. K. Sasaki, N. Nafarizal, Enhancement of Ti^+ density in high-pressure magnetron sputtering plasmas. J. Phys. D Appl. Phys. **43**(12), 124012 (2010)
33. K. Shibagaki, N. Nafarizal, K. Sasaki, Spatial distribution of the velocity distribution function of Fe atoms in a magnetron sputtering plasma source. J. Appl. Phys. **98**(4), 043310 (2005)
34. P. Sigmund, Theory of sputtering. I. Sputtering yield of amorphous and polycrystalline targets. Phys. Rev. **184**(2), 383–416 (1969)
35. N.M. Šišović, N.V. Ivanović, G.L. Majstorović, N. Konjević, Ne I spectral line shapes in Grimm-type glow discharge. J. Anal. At. Spectrom. **29**(11), 2058–2063 (2014)
36. Dj. Spasojević, M. Cvejić, N.M. Šišović, N. Konjević, Simultaneous plasma and electric field diagnostics of microdischarge from hydrogen Balmer line shape. Appl. Phys. Lett. **96**, 241501 (2010)
37. Dj. Spasojević, N.V. Ivanović, N.V. Nedić, N.M. Šišović, N. Konjević, Complex UV Ne II line shapes in the cathode sheath of an abnormal glow discharge. Plasma Sources Sci. Technol. **29**, 085008 (2020)
38. Dj. Spasojević, S. Mijin, N.M. Šišović, N. Konjević, Spectroscopic application of an iterative kinetic cathode sheath model to high voltage hollow cathode glow discharge in hydrogen. J. Appl. Phys. **119**(5), 053301 (2016)
39. Dj. Spasojević, V. Steflekova, N.M. Šišović, N. Konjević, Spectroscopic application of an iterative kinetic model of the cathode-fall region in a hydrogen abnormal glow discharge. Plasma Sources Sci. Technol. **23**(1), 012004 (2014)
40. Dj. Spasojević, V. Steflekova, N.M. Šišović, N. Konjević, Electric field distribution in the cathode-fall region of an abnormal glow discharge in hydrogen: experiment and theory. Plasma Sources Sci. Technol. **21**(2), 025006 (2012)
41. M.M. Vasiljević, Dj. Spasojević, N.M. Šišović, N. Konjević, Stark effect of Ar I lines for electric field strenght diagnostics in the cathode sheath of glow discharge. Europhys. Lett. **119**(5), 55001 (2017)
42. M.M. Vasiljević, Đ Spasojević, N. Konjević, Study of the Ar II spectral line shape in the cathode sheath region of glow discharge. AIP Adv. **11**, 035137 (2021)
43. I.R. Videnović, N. Konjević, M.M. Kuraica, Spectroscopic investigaions of a cathode fall region of the Grimm-type glow discharge. Spectrochim. Acta Part B **51**(13), 1707–1731 (1996)
44. A. von Engel, *Ionized gases* (Clarendon Press, Oxford, 1965)
45. T. Wujec, H.W. Janus, W. Jeleński, Spectroscopic measurements of electric field distributions in dielectric barrier discharges in hydrogen. J. Phys. D Appl. Phys. **36**(7), 868–877 (2003)
46. Y. Yamamura, M. Ishida, Monte Carlo simulation of the thermalization of sputtered atoms and reflected atoms in the magnetron sputtering discharge. J. Vac. Sci. Technol. A **13**(1), 101–112 (1995)
47. J. F., Ziegler, M. D., Ziegler,J. P., Biersack, SRIM-2008 (2008) <www.SRIM.org>